Title	Mn-doping-induced itinerant-electron ferromagnetism in Cr[2]GeC
Author(s)	Liu, Z.; Waki, T.; Tabata, Y.; Nakamura, H.
Citation	Physical Review B (2014), 89(5)
Issue Date	2014-02-28
URL	http://hdl.handle.net/2433/187045
Right	©2014 American Physical Society
Type	Journal Article
Textversion	publisher

Mn-doping-induced itinerant-electron ferromagnetism in Cr_2GeC

Z. Liu, T. Waki, Y. Tabata, and H. Nakamura*

Department of Materials Science and Engineering, Kyoto University, Kyoto 606-8501, Japan

(Received 20 November 2013; revised manuscript received 9 February 2014; published 28 February 2014)

The magnetism of the $M_{n+1}AX_n$ phase, Cr_2GeC, and its Mn-doped system, $(Cr_{1-x}Mn_x)_2GeC$ ($x \leqslant 0.25$), synthesized via a solid state reaction, was investigated systematically. Cr_2GeC is in a spin-unpolarized state, but the ferromagnetic band polarization is induced immediately by the Mn doping. The Curie temperature, T_C, and the spontaneous moment, p_s, increase almost proportionally to the Mn concentration, strongly suggesting that Cr_2GeC is located in the vicinity of a ferromagnetic quantum critical point. The strong concentration dependence of p_{eff}/p_s, where p_{eff} is the effective moment in the paramagnetic state, indicates that the ferromagnetism appearing in the Mn-doped Cr_2GeC can be classified as a typical itinerant-electron ferromagnetism in a wide range of the degree of electron localization.

DOI: 10.1103/PhysRevB.89.054435 PACS number(s): 75.10.Lp, 71.20.Be, 75.50.Cc

I. INTRODUCTION

A class of ternary hexagonal compounds $M_{n+1}AX_n$ ($n = 1,2,3,\ldots$; space group $P6_3/mmc$, abbreviated as MAX), where M is an early transition metal, A an A-group element (mostly IIIA and IVA), and X usually C and/or N, has attracted extensive attention because their nanolaminate structure results in unique mechanical, physical, and chemical properties such as the combination of metallic and ceramic characteristics [1–5]. Recently, the addition of magnetic functions to the MAX phases has aroused considerable interest from a number of researchers. Possible spin polarization in MAX phases, such as Cr_2AlC [6–8], Cr_2GeC [9–13], hypothetical $Fe_{n+1}AC_n$ [14], and $(Cr_{1-x}Mn_x)_2AlC$ [15], has been suggested theoretically. Experimental efforts to find magnetic phases have also been made in $(Cr_{1-x}Mn_x)_2AlC$ [16] and $(Cr_{1-x}Mn_x)_2GaC$ [17], and the discovery of room-temperature ferromagnetism in single-crystalline thin-film $(Cr_{0.75}Mn_{0.25})_2GeC$, designed based on theoretical prediction, has been reported just recently [18]. The present authors have found a spin-density-wave transition in Cr_2GaN at $T_N = 170$ K [19].

Some theoretical works have predicted that Cr_2GeC is spin polarized in the ground state [9–13]. In the present paper, we characterize the actually spin-unpolarized ground state in Cr_2GeC and discuss the nature of the electronic state, namely, the proximity to the ferromagnetic quantum criticality, in the conventional framework of metallic magnetism. Furthermore, because the room-temperature ferromagnetism found in thin-film $(Cr_{0.75}Mn_{0.25})_2GeC$ [18] seems to be characterized further, we made a systematic study of Mn-doped Cr_2GeC synthesized via a simple solid-state reaction to interpret the ferromagnetism appearing as a result of the Mn doping from the viewpoint of fundamental magnetism, just like the Al-doping-induced ferromagnetism in the correlated-electron metal YCo_2 [20]. We apply Takahashi's theory of spin fluctuations [21] to describe the typical itinerant-electron ferromagnetism.

II. EXPERIMENTAL PROCEDURES

Polycrystalline samples of $(Cr_{1-x}Mn_x)_2GeC$ ($0 \leqslant x \leqslant 0.25$) were synthesized through a solid-state reaction with constituent elements of Cr (99.9% pure 100 mesh powder), Mn (99.9% pure 200 mesh powder), Ge (99.999% pure 6- to 20-mm flakes), and C (99.95% pure 200 mesh pure) purchased from the Rare Metallic Co., Ltd. The starting materials were mixed in desired proportions, sealed in evacuated quartz tubes, and heated at 950 °C for 24 h and then at 1000 °C for 48 h. Powder x-ray diffraction (XRD) studies were performed at room temperature using an x-ray diffractometer (Rigaku, Mini-flex) with Cu $K\alpha$ radiation. Magnetic properties were measured by using a SQUID magnetometer (MPMS, Quantum Design) installed at the Research Center for Low Temperature and Materials Science, Kyoto University, in the temperature range of 2–350 K and under magnetic fields of up to 5 T.

III. RESULTS

Cr_2GeC is known to form the Cr_2AlC-type MAX-phase crystal structure [22], whereas no stable Mn_2GeC compound with the same structure has been reported. XRD profiles of $(Cr_{1-x}Mn_x)_2GeC$ ($0 \leqslant x \leqslant 0.25$) are shown in Fig. 1. The main phase is identified as the MAX phase with the Cr_2AlC-type structure, indicating that we succeeded in Mn-doping to Cr_2GeC up to $x \simeq 0.25$. At $x \geqslant 0.2$, however, we detected the presence of appreciable impurity phases; the most probable impurity phase is $Mn_{11}Ge_8$. Hence, the solubility limit is estimated to be $x \sim 0.25$. Figure 2 shows Mn concentration dependencies of lattice parameters a and c at room temperature; the parameters increase slightly at low Mn contents and decrease at high Mn contents. The value of c/a is nearly constant within 4.10 ± 0.09. Because there is no Mn_2GeC, it is difficult to discuss the origin of this nonlinear behavior. Such an anomalous deviation from Vegard's law is occasionally observed in the poor-Mn-doping region in a solid solution of intermetallics [23].

Figure 3 shows temperature dependencies of the susceptibility measured for nondoped Cr_2GeC. Results of Cr_2GaC [19] and Cr_2AlC (unpublished) are also included for comparison. Weak temperature dependencies are typical for Pauli paramagnetic metals. Upturns seen at low temperatures are

*nakamura.hiroyuki.2w@kyoto-u.ac.jp

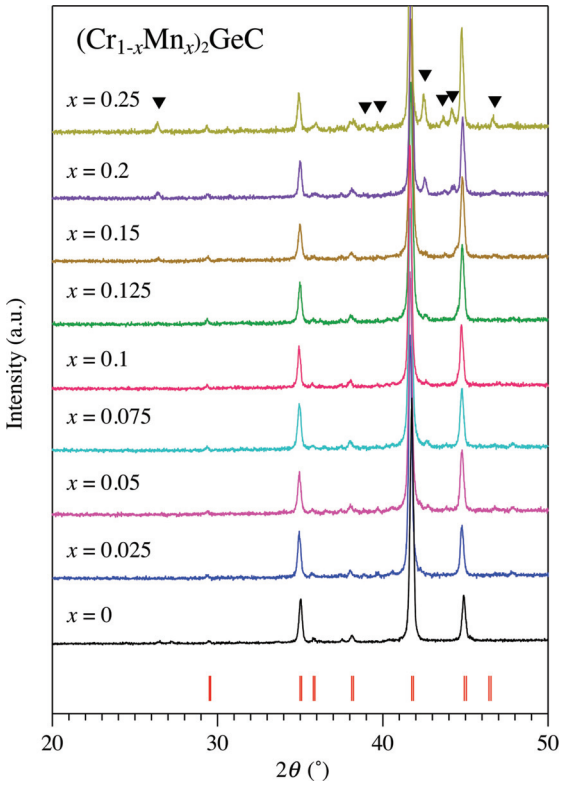

FIG. 1. (Color online) Examples of room-temperature XRD profiles of $(Cr_{1-x}Mn_x)_2GeC$ ($0 \leqslant x \leqslant 0.25$). Close arrowheads represent diffractions from $Mn_{11}Ge_8$. Vertical bars stand for peak positions expected for pure Cr_2GeC with the Cr_2AlC structure.

ascribed to paramagnetic impurities. To show no spontaneous magnetization, magnetization curves at 2 K are also shown in the inset in Fig. 3; the slight nonlinearity is ascribed to impurity contributions. The absolute magnitude of the susceptibility increases from Cr_2AlC to Cr_2GeC, indicating that Cr_2GeC is the most enhanced magnetically in the Cr_2AC series.

Figures 4(a) and 4(b) show typical temperature dependencies of the magnetization measured at 1 T and magnetization curves at 2 K, respectively, for Mn-doped Cr_2GeC. Clearly ferromagnetism appears with Mn doping, and the Curie

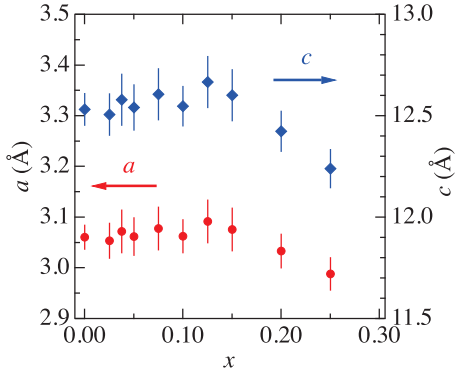

FIG. 2. (Color online) Mn concentration dependencies of lattice parameters a and c of $(Cr_{1-x}Mn_x)_2GeC$ ($0 \leqslant x \leqslant 0.25$) at room temperature.

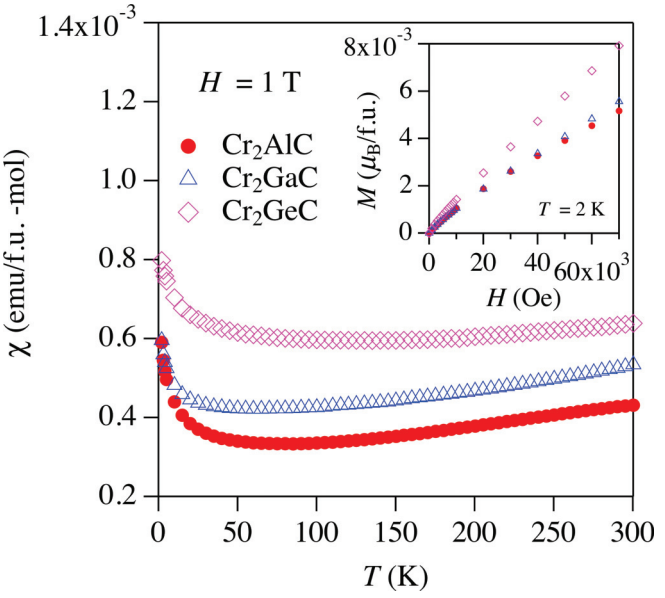

FIG. 3. (Color online) Temperature dependencies of the susceptibility for Cr_2GeC, Cr_2GaC, and Cr_2AlC. The data are taken from Ref. [19]. The inset shows the magnetization curves at 2 K.

temperature, T_C, and the spontaneous magnetization, p_s, increase with Mn doping. One may doubt the effect of impurities. In fact, the most probable impurity phase, $Mn_{11}Ge_8$, orders ferromagnetically below $T_C = 274$ K followed by a successive antiferromagnetic transition at $T_N = 150$ K [24]. The magnetization of $Mn_{11}Ge_8$ is, however, 7 emu/g at its

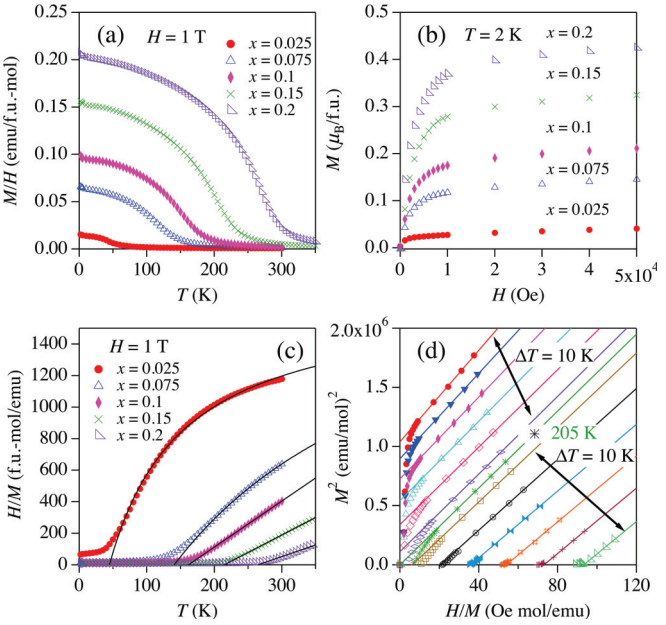

FIG. 4. (Color online) Examples of temperature dependencies of the magnetization measured at 1 T (a), magnetization curves at 2 K (b), and temperature dependencies of H/M (c) for $(Cr_{1-x}Mn_x)_2GeC$. Solid lines in panel (c) represent the fit to Eq. (1). (d) M^2 versus H/M plot for $(Cr_{0.85}Mn_{0.15})_2GeC$ at various temperatures.

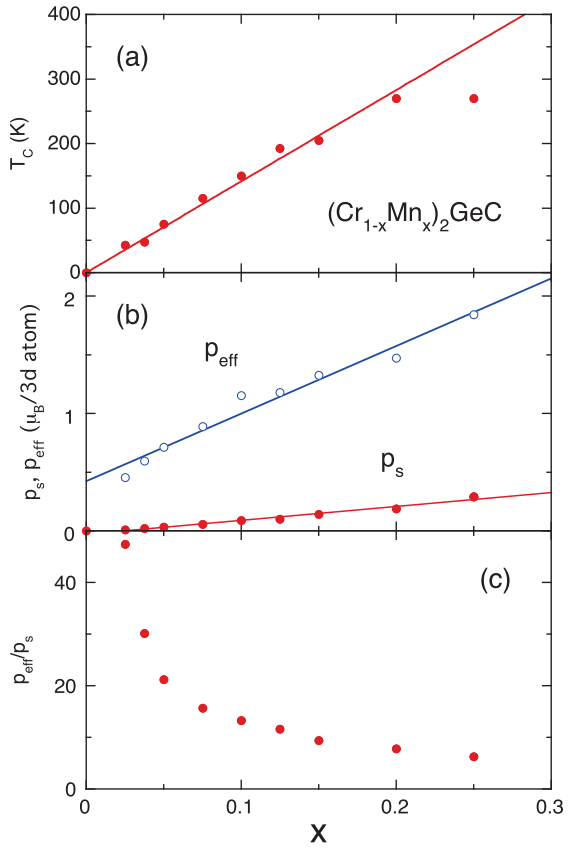

FIG. 5. (Color online) Mn concentration dependencies of T_C (a), spontaneous moment p_s and effective moment p_{eff} per magnetic atom (b), and p_{eff}/p_s (c) for $(Cr_{1-x}Mn_x)_2GeC$ ($x \leqslant 0.25$).

maximum. Even if we assume 10% inclusion of $Mn_{11}Ge_8$, its contribution accounts for only <3% of the experimentally observed magnetization of $(Cr_{0.80}Mn_{0.20})_2GeC$. Therefore we can safely conclude that the ferromagnetism is an intrinsic property of the Mn-doped MAX phases.

Usually, to determine the reliable value of T_C of a ferromagnet, an $M(T,H)^2$ versus $H/M(T,H)$ plot (the so-called Arrott plot) is applied. Figure 4(d) shows M^2 plotted against the H/M plot for $(Cr_{0.85}Mn_{0.15})_2GeC$ near T_C. Straight lines in the figure indicate linear fits to high-field parts. From this analysis, we estimate $T_C = 205$ K, which agrees well with the temperature at which the temperature derivative of magnetization, dM/dT [at 1 T, Fig. 4(a)], takes a minimum.

T_C estimated from dM/dT (at 1 T) is plotted as a function of Mn concentration x in Fig 5(a) and the values are listed in Table I. Ferromagnetic order appears from zero Mn concentration and T_C increases almost linearly to x. T_C saturates at $x \sim 0.2$. Considering the fact that the compound with $x = 0.25$ includes appreciable impurities, T_C of the Mn-doped Cr_2GeC system reaches a maximum at $x =$ 0.2–0.25. The room-temperature ferromagnetism observed in thin-film $(Cr_{0.75}Mn_{0.25})_2GeC$ [18] roughly accords with our observation. We estimate the spontaneous magnetic moment p_s per magnetic atom (Mn and Cr) from a linear extrapolation of M^2 to $H = 0$ in the M^2 versus H/M plot at 2 K, and we plot it as a function of x in Fig. 5(b). p_s nearly scales as T_C.

TABLE I. Parameters for $Cr_{1-x}Mn_xGeC$ with $0 \leqslant x \leqslant 0.25$.

x	T_C (K)	p_s (μ_B/3d atom)	p_{eff} (μ_B/3d atom)	T_0 (10^4 K)	T_A (10^4 K)
0.0	0	0			
0.025	43	0.010	0.456	3.25	101
0.0375	48	0.020	0.596	1.62	34.9
0.05	75	0.034	0.712	1.54	22.6
0.075	115	0.057	0.888	1.51	14.1
0.10	150	0.087	1.15	1.46	8.68
0.125	192	0.101	1.18	1.81	8.23
0.15	205	0.140	1.33	1.42	5.08
0.20	270	0.189	1.47	1.55	3.93
0.25	270	0.292	1.84	1.24	1.77

The susceptibility above T_C was fitted to the modified Curie-Weiss law,

$$\chi = \frac{C}{T-\theta} + \chi_0, \quad (1)$$

where C is the Curie constant, θ the paramagnetic Curie temperature, and χ_0 a temperature-independent term. The fit is represented by solid curves in Fig. 4(c). The effective magnetic moment, p_{eff}, per magnetic atom is estimated from $C = N\mu_B^2 p_{eff}^2/3k_B$, where N is the number of magnetic atoms, μ_B the Bohr magneton, and k_B the Boltzmann constant. p_{eff} is plotted against x in Fig. 5(b) and is seen to vary nearly linearly.

The Mn concentration dependence of p_{eff}/p_s is shown in Fig. 5(c). When x is small, p_{eff}/p_s is much larger than unity, indicating that the compound is in the regime of a very weak itinerant-electron ferromagnet. p_{eff}/p_s decreases rapidly with increasing x and approaches the local moment limit. This concentration dependence demonstrates that the Mn-doped Cr_2GeC is a typical itinerant electron system covering different degrees of electron localization. Needless to say, the possibility of a localized moment only at the Mn site can be excluded.

IV. DISCUSSION

A. Proximity to the quantum criticality of Cr_2GeC

In Cr_2AC (A = Ge, Ga, Al), experimental observation indicates no spontaneous magnetization down to the lowest temperature. The absence of a phase transition of Cr_2GeC in the temperature range of 3–1500 K has already been confirmed in specific heat measurements [25]. There is also no microscopic evidence of long-range magnetic ordering in Cr_2GaC and Cr_2AlC from Ga and Al nuclear magnetic resonance experiments, respectively [19,26]. In addition, the increase of T_C in proportion to Mn concentration indicates that the long-range ordering is completely suppressed in nondoped Cr_2GeC. These experimental results clearly exclude the possibility of antiferromagnetism as well as ferro- and ferrimagnetism. The discordance with spin-polarized ground states predicted by electronic structure calculations [9–13] is probably because those calculations failed to take into

account the effect of spin fluctuations, as often encountered in strongly correlated electron systems. Hence, we can conclude convincingly that Cr_2GeC is in a spin-unpolarized state throughout the temperature range.

Results of band structure calculations [9–13,27–30] tell us that Cr_2GeC is a typical metal in the sense that Cr-3d bands dominate the density of states at the Fermi level, $D(E_F)$. The systematic increase of χ from Cr_2AlC to Cr_2GeC is understood as the increase in $D(E_F)$ and/or exchange enhancement. The comparison of the electronic specific heat coefficient, γ, of Cr_2AlC [31,32] and Cr_2GeC [25] leads to the same discussion. The relatively large γ value (and χ) means that Cr_2GeC is exchange enhanced. At low temperatures, the temperature coefficient of the electrical resistivity of Cr_2GeC is larger than that of Cr_2AlC [33]. This fact is also interpreted in the same context. These results indicate that Cr_2GeC can be classified as a correlated-electron paramagnetic metal. If this is the case, the mass enhancement of Cr_2GeC compared with bare $D(E_E)$ by a factor of 3, pointed out in Ref. [34], is not surprising. In a classical rigid band picture, the appearance of the ferromagnetism by the Mn doping, i.e., electron doping, is understood as the increase of $D(E_F)$ to satisfy the Stoner criterion; $D(E_F)$ of spin-unpolarized Cr_2GeC is located at the low-energy side of a sharp peak of the density of states [27–30].

It is worth noting the fact that, in the Mn-doped Cr_2GeC system, T_C approaches zero almost proportionally to the Mn concentration. This fact strongly suggests that Cr_2GeC is located in the vicinity of the quantum critical point. In other words, the band polarization, suppressed in nondoped Cr_2GeC, is promptly induced by a small perturbation, i.e., a slight Mn doping just like Al doping to YCo_2 [20]. In fact, T_C in Fig. 5(a) may be slightly overestimated, as is discussed in the next section. The real quantum critical point may be present for a slightly Mn-doped sample. The search for non-Fermi liquid behaviors at lower temperatures appears to be of interest in the Cr_2GeC system.

B. Analysis by the spin fluctuation theory

In theories of the itinerant-electron magnetism initiated by the self-consistent renormalization (SCR) theory of spin fluctuations [35], the dynamical spin fluctuation spectrum is characterized by two parameters, T_0 and T_A, which represent the distribution widths in energy and wave-vector spaces, respectively. In the theories, the coefficient of the M^4 term of the Landau expansion of free energy is one of the most important parameters, called $\bar{F}_1$, which is usually related to the slope of Arrott plot ζ as

$$\bar{F}_1 = N^3(g\mu_B)^4/\zeta, \tag{2}$$

where g is Landé's g factor.

Takahashi [21] developed the theory of spin fluctuations by assuming global conservation of the spin amplitude including zero-point and thermal fluctuations. It is known that his theory is useful for describing itinerant-electron systems particularly with ferromagnetic electron correlations. According to his theory, spectral parameters, T_A and T_0, are estimated from experimental values of $\bar{F}_1$, p_s, and T_C with the use of the

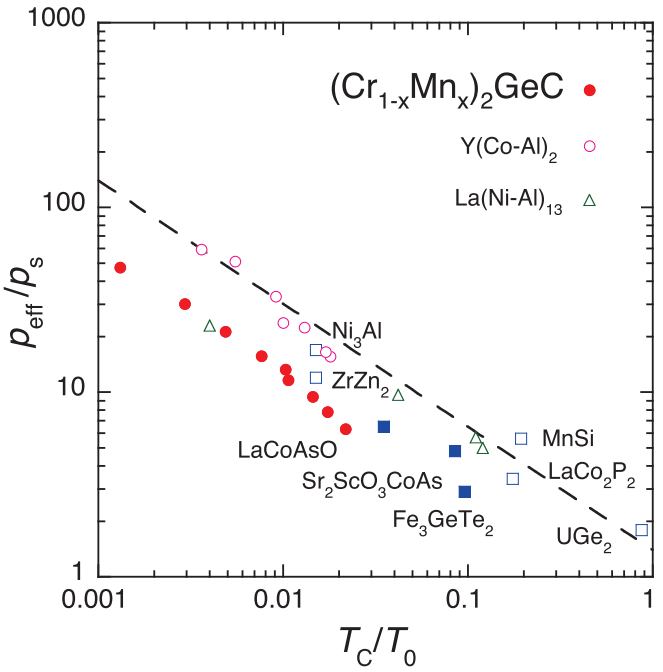

FIG. 6. (Color online) Deguchi-Takahashi plot, i.e., p_{eff}/p_s versus T_C/T_0 plot on logarithmic scales, for $(Cr_{1-x}Mn_x)_2GeC$ with $0 < x \leqslant 0.25$. Equation (5) is shown by the broken line. See Ref. [21] for details. The p_{eff}/p_s values of $(Cr_{1-x}Mn_x)_2GeC$ appear to be smaller than those of Eq. (5) probably due to the two dimensionality of this system. Reported data of two-dimensional itinerant-electron magnets, Sr_2ScO_3CoAs, LaCoAsO [37], and Fe_3GeTe_2 [38], are also included for comparison.

theoretical relations

$$p_s^2 = \frac{20T_0}{T_A}C_{4/3}\left(\frac{T_C}{T_0}\right)^{4/3}, \quad C_{4/3} = 1.006\,089\ldots, \tag{3}$$

$$\bar{F}_1 = \frac{2T_A^2}{15cT_0}, \tag{4}$$

where c is a constant ($c = 0.5$). Values of T_A and T_0 estimated for $(Cr_{1-x}Mn_x)_2GeC$ with $0 < x \leqslant 0.25$ are listed in Table I.

By using experimentally obtained T_0, values of p_{eff}/p_s are plotted against T_C/T_0 in logarithmic scales in Fig. 6. This plot corresponds to an extended version of the Rhodes-Wohlfarth plot [36], which was modified by Takahashi and is known as the Deguchi-Takahashi plot [21]. As is seen in the figure, a number of typical itinerant-electron ferromagnets follow the relation

$$\frac{p_{eff}}{p_s} = 1.4\left(\frac{T_C}{T_0}\right)^{-2/3} \tag{5}$$

derived in Takahashi's theory. The values of p_{eff}/p_s for the Mn-doped Cr_2GeC system are slightly smaller than those expected from this relation. This may be ascribed to the two-dimensionality inherent to the layered crystal structure of this system; Takahashi [21] has already discussed that a smaller p_{eff}/p_s is expected with decreasing dimensionality for the same T_C/T_0. Similar observations have been reported for two-dimensional itinerant-electron magnets such as Sr_2ScO_3CoAl, LaCoAsO [37], and Fe_3GeTe_2 [38]. This fact manifests that the

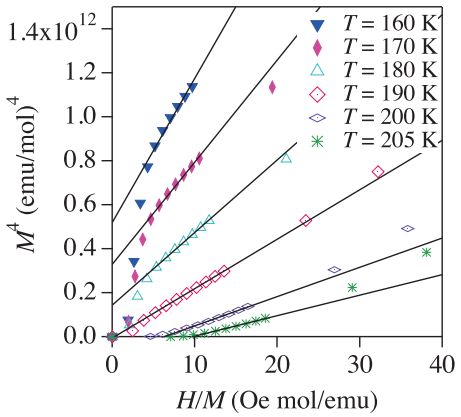

FIG. 7. (Color online) M^4 versus H/M plot for $(Cr_{0.85}Mn_{0.15})_2GeC$ at several temperatures near T_C.

Mn-doped Cr_2GeC system is a prototypical itinerant-electron ferromagnetic system ranging from a weak limit to a relatively well-localized regime.

In Takahashi's theory, a linear relation between M^4 and H/M is predicted at the critical temperature T_C as a ferromagnetic critical behavior. Figure 7 shows M^4 plotted against H/M for $(Cr_{0.85}Mn_{0.15})_2GeC$. The M^4 plot works well just near $T_C \simeq 190$ K, as predicted by the theory. The value of T_C is a little smaller than that estimated by the high-field extrapolation in the conventional M^2 versus H/M Arrott plot.

V. CONCLUSION

We succeeded in synthesizing Mn-doped MAX phase compounds, $(Cr_{1-x}Mn_x)_2GeC$, in the Mn concentration range of $0 \leqslant x \leqslant 0.25$, via a solid-state reaction. Nondoped Cr_2GeC is in a spin-unpolarized state but lies close to the ferromagnetic quantum criticality. The Mn doping induces ferromagnetic band polarization, where T_C and p_s increase nearly proportionally to the Mn concentration. T_C reaches around room temperature at $x \sim 0.2$, being consistent with the finding in the single-crystalline thin film [18]. The ferromagnetism appearing in Mn-doped Cr_2GeC is understood as a prototypical itinerant-electron ferromagnetism ranging from a very weak limit to a relatively electron-localized regime.

[1] M. W. Barsoum, Prog. Solid State Chem. **28**, 201 (2000).
[2] J. Y. Wang and Y. C. Zhou, Annu. Rev. Mater. Res. **39**, 415 (2009).
[3] P. Eklund, M. Beckers, U. Jansson, H. Högberg, and L. Hultman, Thin Solid Films **518**, 1851 (2010).
[4] Z. Sun, H. Hashimoto, W. Tian, and Y. Zou, Int. J. Appl. Ceram. Technol. **7**, 704 (2010).
[5] M. Radovic and M. W. Barsoum, Am. Ceram. Soc. Bull. **92**, 20 (2013).
[6] Y. L. Du, Z. M. Sun, H. Hashimoto, and M. W. Barsoum, J. Appl. Phys. **109**, 063707 (2011).
[7] M. Ramzan, S. Lebgue, and R. Ahuja, Phys. Status Solidi RRL **5**, 122 (2011).
[8] M. Dahlqvist, B. Alling, and J. Rosn, J. Appl. Phys. **113**, 216103 (2013).
[9] W. Zhou, L. Liu, and P. Wu, J. Appl. Phys. **106**, 033501 (2009).
[10] M. Mattesini and M. Magnuson, J. Phys.: Condens. Matter **25**, 035601 (2013).
[11] M. Ramzan, S. Lebegue, and R. Ahuja, Solid State Commun. **152**, 1147 (2012).
[12] N. Li, C. C. Dharmawardhana, K. L. Yao, and W. Y. Ching, Solid State Commun. **174**, 43 (2013).
[13] H. I. Faraoun, F. Z. Abderrahim, and C. Esling, Comput. Mater. Sci. **74**, 40 (2013).
[14] W. Luo and R. Ahuja, J. Phys.: Condens. Matter **20**, 064217 (2008).
[15] M. Dahlqvist, B. Alling, I. A. Abrikosov, and J. Rosen, Phys. Rev. B **84**, 220403 (2011).
[16] A. Mockute, M. Dahlqvist, J. Emmerlich, L. Hultman, J. M. Schneider, P. O. Å. Persson, and J. Rosen, Phys. Rev. B **87**, 094113 (2013).
[17] S. Lin, P. Tong, B. S. Wang, Y. N. Huang, and W. J. Lu, J. Appl. Phys. **113**, 053502 (2013).
[18] A. S. Ingason, A. Mockute, M. Dahlqvist, F. Magnus, S. Olafsson, U. B. Arnalds, B. Alling, I. A. Abrikosov, B. Hjörvarsson, P. O. Å. Persson, and J. Rosen, Phys. Rev. Lett. **110**, 195502 (2013).
[19] Z. Liu, T. Waki, Y. Tabata, K. Yuge, H. Nakamura, and I. Watanabe, Phys. Rev. B **88**, 134401 (2013).
[20] K. Yoshimura and Y. Nakamura, Solid State Commun. **56**, 767 (1985).
[21] Y. Takahashi, *Spin Fluctuation Theory of Itinerant Electron Magnetism*, Springer Tracts in Modern Physics Vol. 253 (Springer, Berlin, 2013).
[22] W. Jeitschko, H. Nowotny, and F. Benesovsky, Monatsh. Chem. **94**, 844 (1963).
[23] M. Shiga, H. Wada, H. Nakamura, K. Yoshimura, and Y. Nakamura, J. Phys. F **17**, 1781 (1987).
[24] N. Yamada, K. Maeda, Y. Usami, and T. Ohoyama, J. Phys. Soc. Jpn. **55**, 3721 (1986).
[25] M. K. Drulis, H. Drulis, A. E. Hackemer, O. Leaffer, J. Spanier, S. Amini, M. W. Barsoum, T. Guilbert, and T. El-Raghy, J. Appl. Phys. **104**, 023526 (2008).
[26] C. S. Lue, J. Y. Lin, and B. X. Xie, Phys. Rev. B **73**, 035125 (2006).
[27] Z. Sun, D. Music, R. Ahuja, S. Li, and J. M. Schneider, Phys. Rev. B **70**, 092102 (2004).
[28] A. Bouhemadou, Appl. Phys. A **96**, 959 (2009).
[29] Z. J. Yang, J. Li, R. F. Linghu, X. S. Song, X. L. Cheng, Z. H. Zhu, and X. D. Yang, Eur. Phys. J. B **86**, 1 (2013).
[30] Z.-Y. Jiao, S.-H. Ma, and X.-F. Huang, J. Alloys Compd. **583**, 607 (2014).
[31] S. E. Lofland, J. D. Hettinger, K. Harrell, P. Finkel, S. Gupta, M. W. Barsoum, and G. Hug, Appl. Phys. Lett. **84**, 508 (2004).
[32] M. K. Drulis, H. Drulis, S. Gupta, M. W. Barsoum, and T. El-Raghy, J. Appl. Phys. **99**, 093502 (2006).
[33] M. W. Barsoum, T. H. Scabarozi, S. Amini, J. D. Hettinger, and S. E. Loflan, J. Am. Ceram. Soc. **94**, 4123 (2011).

[34] P. Eklund, M. Bugnet, V. Mauchamp, S. Dubois, C. Tromas, J. Jensen, L. Piraux, L. Gence, M. Jaouen, and T. Cabioc'h, Phys. Rev. B **84**, 075424 (2011).

[35] T. Moriya, *Spin Fluctuations in Itinerant Electron Magnetism*, Springer Series in Solid State Sciences Vol. 56 (Springer, Berlin, 1985).

[36] P. Rhodes and E. P. Wohlfarth, Proc. R. Soc. London, Ser. A **273**, 247 (1963).

[37] H. Ohta, D. Noguchi, K. Nabetani, and H. A. Katori, Phys. Rev. B **88**, 094441 (2013).

[38] B. Chen, J. Yang, H. Wang, M. Imai, H. Ohta, C. Michioka, K. Yoshimura, and M. Fang, J. Phys. Soc. Jpn. **82**, 124711 (2013).